Published in final edited form as:
Dev Dyn. 2012 November ; 241(11): 1770–1781. doi:10.1002/dvdy.23866.

Non-Muscle Myosin II Regulation of Lung Epithelial Morphology

Erin J. Plosa[a], **Kimberly A. Gooding**[c], **Roy Zent**[b,c], and **Lawrence S. Prince**[a,c]

[a]Department of Pediatrics, Vanderbilt University School of Medicine, Nashville, TN, 37232

[b]Department of Medicine, Vanderbilt University School of Medicine, Nashville, TN, 37232

[c]Department of Cell and Developmental Biology, Vanderbilt University School of Medicine, Nashville, TN, 37232

Abstract

Background—The regulation of epithelial cell shape and orientation during lung branching morphogenesis is not clearly understood. Non-muscle myosins regulate cell size, morphology, and planar cell polarity. Here we test the hypothesis that non-muscle myosin II (NM II) regulates lung epithelial morphology in a spatially restricted manner.

Results—Epithelial cell orientation at airway tips in fetal mouse lungs underwent a significant transformation at E17. Treatment of E15 lung explants with the NM II inhibitor blebbistatin increased airway branching, epithelial cell size, and the degree of anisotropy in epithelial cells lining the airway stalks. In cultured MLE-12 lung epithelial cells, blebbistatin increased cell velocity, but left the migratory response to FGF-10 unchanged.

Conclusions—In the developing lung, NM II acts to constrain cell morphology and orientation, but may be suppressed at sites of branching and cell migration. The regulation of epithelial orientation may therefore undergo dynamic variations from E15 to E17.

Keywords

bronchopulmonary dysplasia; lung development; epithelial migration; branching morphogenesis; fibroblast growth factor

Introduction

The organization of epithelial cells into 3-dimensional structures gives form and function to developing organs. During formation of branched organs such as the lungs, kidney, salivary gland, and mammary gland, hollow tubes lined by epithelial sheets undergo multiple rounds of branching and division (Hogan, 1999; Srinivas et al., 1999; Affolter et al., 2003; Larsen et al., 2003; Veltmaat et al., 2003; Watanabe and Costantini, 2004; Metzger et al., 2008). Tube branching produces organs with complex structures and large luminal surface areas. Within developing organs, epithelial cells receive spatial and temporal cues that instruct the cells regarding their relative position and orientation. Apical-basal polarity allows vectorial transport across tight epithelial monolayers, and planar cell polarity orients cells with respect to the dorsal-ventral, anterior-posterior, and proximal-distal axes (Lawrence and Shelton, 1975; Vinson and Adler, 1987; Cao et al., 2012; Cho et al., 2012). While the molecular machinery controlling epithelial cell orientation is conserved throughout biology, dynamic

Address Correspondence to: Lawrence S. Prince, MD, PhD, 1115D Light Hall, MRBIV, 2215B Garland Avenue, Nashville, TN 37232, Phone: 615-322-6220, Fax: 615-343-6182, Lance.prince@vanderbilt.edu.

regulation of cell shape and movement produces the unique 3-dimensional structures within individual organs (Klein and Mlodzik, 2005).

Initially formed from simple endoderm, the developing lung epithelium undergoes extensive branching morphogenesis followed by differentiation into specialized cell populations. During the embryonal, pseudoglandular, and early canalicular stages, a simple cuboidal epithelium lines branching airways (Burri, 1984). As lung development progresses from the late canalicular stage through the saccular stage, branching morphogenesis completes while epithelial differentiation begins. In larger airways, epithelial cells differentiate into mucus-producing goblet cells, clara cells, and ciliated cells. The epithelium in the largest airways also becomes pseudostratified, with basal cells found against the basement membrane (Mercer et al., 1994). In the distal lung, type I epithelial cells flatten and enlarge to eventually cover most of the alveolar surface area (Burri, 1984). Type II epithelial cells begin expressing surfactant proteins critical for lung function following birth. How cells regulate morphology and orientation in the context of differentiation is unclear.

Defects in airway branching morphogenesis during the later canalicular and saccular stages of lung development contribute to the pathogenesis of bronchopulmonary dysplasia, the most common serious morbidity affecting preterm infants (Christou and Brodsky, 2005; MacDorman et al., 2005; Mathews and MacDorman, 2011). We have previously established a late stage explant model to test the molecular and cellular mechanisms regulating airway formation (Prince et al., 2004; Prince et al., 2005; Benjamin et al., 2009; Benjamin et al., 2010; Blackwell et al., 2011). In E15-E16 fetal mouse lung explants, inflammatory mediators and NF-κB activation inhibit expression of FGF-10, a key growth factor that drives epithelial migration at the tips of airways and stimulates eventual branch formation (Benjamin et al., 2010). However, many basic molecular mechanisms regulating the formation of new airway branches in the later stage mouse lung remain unknown.

Coordinated movement of epithelial cells requires the intracellular actin and myosin containing cytoskeleton. Actin containing stress fibers provide mechanical tension. Non-muscle myosins provide the ATP-dependent active force required both for cell migration and maintenance of cell shape and orientation (Lo et al., 2004; Betapudi et al., 2006; Vicente-Manzanares et al., 2007). Myosin II contains two heavy chains and two pairs of regulatory light chains and function as ATP-dependent motor proteins. Phosphorylation of the myosin heavy chain drives the power stroke between myosin and actin stress fibers (Vicente-Manzanares et al., 2009). The lung expresses three non-muscle myosin II heavy chain subunits with varied roles in embryogenesis and development (Wang et al., 2011). Mice lacking NM II-A die at embryonal day 6.5 (E6.5) with major defects in cell adhesion and endoderm formation (Conti et al., 2004). NM II-B knockout mice display significant heart and brain abnormalities and die at E14 while mice lacking NM II-C appear normal (Takeda et al., 2003; Golomb et al., 2004; Ma et al., 2010). The small molecule blebbistatin specifically inhibits function of NM II isoforms (Straight et al., 2003; Limouze et al., 2004). Functional redundancy makes genetic elucidation of each NM II isoform difficult. However, with inhibition of all three isoforms, blebbistatin allows specific, mechanistic insight. Developmental studies using blebbistatin have demonstrated that NM II plays a role in regulating oligodendrocyte branching, neuronal polarity, and intestinal epithelial cell shape (Straight et al., 2003; Limouze et al., 2004; Ivanov et al., 2008; Wang et al., 2008; Wylie and Chantler, 2008; Kollins et al., 2009). Here we used multiple approaches to characterize lung epithelial cell orientation at specific sites along the developing airway and test the role of NM II in regulated epithelial orientation and airway branching during the canalicular and saccular stages of lung development.

Results

Epithelial cell orientations at the canalicular-saccular stage transition

Canalicular stage fetal mouse lungs transition to the saccular stage between E16 and E17 (Ten Have-Opbroek, 1981; Cardoso, 2000). In the saccular stage, distal epithelia differentiate into Type I and Type II cells. During the transition to the saccular stage, airway branching becomes more random and less uniform (Schreider and Raabe, 1981). In humans, defective saccular stage branching contributes to bronchopulmonary dysplasia and other clinically important examples of pulmonary hypoplasia (Christou and Brodsky, 2005). To better understand how epithelial cell orientations change during the transition between the canalicular and saccular stages, we specifically examined cell orientation at the tips of branching airways in E15, E16, and E17 fetal mouse lungs. Immunostaining whole lung lobes for E-cadherin, a transmembrane protein known to interact with adherens junctions subjacent to tight junctions, clearly identified lateral membranes (Figure 1A) of epithelial cells lining the airways (Green et al., 2010; Tian et al., 2011). Analysis of confocal sections obtained at the very tips of airways and perpendicular to the airway stalk axes (Figure 1B) demonstrated three distinct patterns of cell arrangement in E15 and E16 lungs (Figure 1C–G). Cells at the leading edge of the airway were most commonly in a tetrahedral arrangement. Less frequently, cells formed a linear row of three or more cells, suggesting a flattening of the tip of the epithelial tube. A smaller population of airways contained a rosette of epithelial cells with a common cell junction between four or more cells. The distribution of epithelial cell arrangements present at the tips of developing airways were similar in E15 and E16 lungs.

Beginning at E17, we observed a significant transformation in epithelial morphology as the distal epithelial cells differentiated. In approximately 40% of E17 airways, changes in epithelial cell differentiation led to a discontinuous cellular arrangement, with cuboidal cells now adjacent to flattened type I cells (Figure 1F,G). Airways in which epithelial cells had not undergone significant changes in differentiation and cell shape retained the similar tetrahedral, row, and rosette distributions measured at E15 and E16. In addition to describing epithelial orientations at the tips of branching airways, we also examined epithelial arrangements along the length of branching airways, from stalk to tip, using frozen sections immunostained for E-cadherin. From this cross-sectional perspective, E15 frozen sections revealed an epithelial monolayer surrounding the airway lumen (Figure1H). However, the epithelial cells in E17 branching airways changed their cellular arrangement. Stalk epithelial cells maintained a monolayer surrounding the lumen, whereas epithelial cells at the tips were no longer connected to the airway lumen, disrupting the epithelial monolayer (Figure 1I). As epithelial differentiation progresses at E18, immunostaining of frozen sections demonstrated T1α expression, a type I cell marker, in epithelial cells that have left the monolayer. However, these cells lack expression of the type II cell marker NKX2-1 (Figure 1J–K). While the cells at the tips of branching airways do not acquire the flattened appearance of type I cells at this stage, they do appear to express a type I marker.

Non-muscle myosin II localization during the saccular stage of lung development

In epithelial cells, non-muscle myosin II (NM II) provides the active force regulating both planar cell polarity and cell shape (Vicente-Manzanares et al., 2007). To examine expression of the three NM II isoforms, II-A, II-B, and II-C, in airway epithelia in the tip and stalk regions of developing fetal airways, we stained frozen sections of fetal mouse lungs from E15 and E18 (Figure 2). NM II-A is expressed similarly in the tip and stalk epithelia of E15 and E18 fetal lungs (Figure 2A, D, G, J). NM II-B is primarily expressed in fetal lung mesenchyme at both E15 and E18 (Figure 2B, E, H, K). NM II-C co-localizes with E-cadherin along the lateral membranes of tip and stalk epithelial cells in E15 and E18

developing airways (Figure 2C, F, I, L). To examine the expression pattern of the three NM II isoforms during the later stages of fetal lung development, we compared frozen sections immunostained for the NM II isoforms from E15, E18, and postnatal day 0 (P0) (Figure 3). NM II-A staining localized to both epithelia and lung mesenchyme, localizing primarily to the subapical and basal regions of airway epithelia at E15 and E18 (Figure 3A-D, S-V). In P0 lungs, NM II-A staining was highest in flattened type I epithelia compared to type II epithelia (Figure 3E-F, W-X). NM II-B staining localized to fetal lung mesenchyme, with low levels of expression detected in airway epithelia at all three developmental time points examined (Figure 3G-L, Y-D'). NM II-C expression was detected in both epithelia and mesenchyme, and co-localized with E-cadherin along the lateral membranes of E15 airway epithelia (Figure 3M-N, E'-F'). Like NM II-A, NM II-C staining in P0 lung seemed to concentrate in flattened type I epithelial cells (Figure 3Q-R, I'-J'). Therefore all three NM II isoforms are expressed in the developing lung, with NM II-A and NM II-C the most abundant in epithelial cells at both the airway tip and stalk regions.

NM II activity regulates airway branching and cell shape

To test the role of NM II on later stage airway morphogenesis, we used the specific non-muscle myosin inhibitor blebbistatin (Limouze et al., 2004). Explants from E15 fetal mouse lungs were first cultured for 18 h to allow the explants to adhere to the permeable support and then treated with blebbistatin. Interestingly, within the first four hours of treatment, blebbistatin increased the number of new airway branches (Figure 4A, C–D). After 18 h of treatment, blebbistatin did not appear to affect the number of new branches, but did cause a dramatic dilation of peripheral airways compared to controls (Figure 4A, B–C). Blebbistatin treatment beyond 24 h caused explants to collapse and flatten, making visualization of airways difficult.

E-cadherin immunostaining of blebbistatin-treated explants also demonstrated changes in epithelial size and shape. Cells lining the tips of blebbistatin-treated airways were larger than controls (Figure 5F). In addition, blebbistatin caused derangement of cell shape and orientation along the stalks of airways. To quantify these changes, we obtained 3-dimensional stacks of confocal images and measured volumetric cell anisotropy. Higher Degrees of Anisotropy values (with maximum value of 1.0) represented increasingly disordered morphology, and lower values (minimum 0) corresponded to a more regular, ordered cell shape. In control airways, stalk epithelial cells had a Degree of Anisotropy value of 0.33 (+/− 0.01, n = 12); blebbistatin treatment increased the Degree of Anisotropy to 0.81 (+/− 0.01, n = 10; $P < 0.05$) (Figure 5C–E). Interestingly, blebbistatin did not change the anisotropy of cells at the tips of explant airways nor the tip epithelial cell orientations (Figure 5A–B, E, G–L).

The changes in epithelial cell shape, orientation, and size did not appear to involve alterations in cell proliferation or differentiation. As demonstrated in phospho-histone H3 (PH3) immunostained explants, this increase in cell size occurred without a significant change in epithelial cell proliferation between control and blebbistatin treated explants (Figure 6A–C). Although these cultured E15 explants have minimal type I and type II cell differentiation, occasional epithelial cells express the type II marker NKX2-1. The number of NKX2-1 positive cells per mm^2 was not different between control and blebbistatin treated explants (Figure 6D–F). Collectively, these explant experiments show that NM II functions to restrict airway branch formation, limit airway size, and maintain regular, ordered epithelial cell shape. However, the effects of blebbistatin appear restricted to specific sites of the branching airway.

NM II inhibition increases epithelial cell migration

Data showing that blebbistatin increased branching and affected cell size and orientation only within airway stalks suggested that NM II might restrict epithelial cells from migrating toward chemoattractant sources. To test the effects of NM II on epithelial cell chemotaxis, we measured migration of MLE-12 cells, which share properties with immature distal airway epithelial cells (Figure 7). The chemoattractant FGF-10 increased both MLE-12 cell velocity and the number of cells that entered an artificial wound (Figure 7). Blebbistatin increased cell velocity both in control and FGF-10 treated cells, without increasing the number of cells leaving the monolayer edge and entering the wound.

Previous studies showed that blebbistatin alters focal contact formation and stability in 3T3 cells (Dumbauld et al., 2010). To test if a similar process could be regulating MLE-12 migration, we visualized both actin-containing focal contacts and sites of tyrosine phosphorylation (Figure 8). In control MLE-12 cells, phosphotyrosine staining localized to focal contacts at the leading edge of membranes in migrating cells. FGF-10 increased phosphotyrosine staining along the membrane periphery, consistent with FGF receptor activation. Blebbistatin treatment alone reduced the number of clearly visible focal contacts, but did not dramatically alter phosphotyrosine staining. Adding FGF-10 to blebbistatin-treated cells increased phosphotyrosine staining at punctate focal contacts throughout the cells, not just at the leading membrane edge (Figure 8D, H). Collectively, these results suggest that NM II functions to constrain epithelial cell morphology and limit migration, but does not inhibit the response to FGF.

Discussion

NM II plays a critical role in controlling cell shape, orientation, and movement (Vicente-Manzanares et al., 2005; Vicente-Manzanares et al., 2007; Yam et al., 2007). Redundancy of the three NM II isoforms makes genetic elucidation of the contribution of each isoform difficult. However, use of the NM II inhibitor blebbistatin provides specific, mechanistic insight into the role of NM II during airway branching. Our data show that NM II functions during lung development to regulate epithelial cell morphology and airway branching. NM II activity along the airway stalks constrains airway caliber and could restrict uncontrolled migration of epithelial cells within or out of the epithelial monolayer. NM II likely exerts its effects on epithelia at specific sites along the developing airway, as blebbistatin increases branching before leading to airway dilation and has different effects on epithelial cells in airway stalks compared to the airway tips. Spatial restriction of NM II function may allow changes in airway morphology at sites of active branching while keeping the size and shape of existing airways relatively constant. Importantly, our data suggest that NM II regulation changes during the later stages of lung morphogenesis, as branching completes and epithelial cells differentiate.

During the early stages of lung morphogenesis, airway branching follows a precise stereotypical pattern (Metzger et al., 2008). These controlled branching events require strict spatial regulation of epithelial cell positioning and orientation. Our data support this idea, as cell orientation at the tips of elongating airways in E15 and E16 mouse lungs is remarkably similar. However, airway morphogenesis at the canalicular-saccular stage transition around E17 uses a less well-defined paradigm. During these later stages of development, airway branching appears more random, with epithelial cells appearing to lose contact with the airway lumen and invading the adjacent mesenchyme. The distal airway epithelia no longer form uniform monolayers, but instead contain both flattened cells and round, cuboidal cells. In the E18 lung, epithelial cells no longer contacting the airway lumen directly expressed the type I cell marker T1α, but not the type II cell marker NKX2-1. The final differentiation phenotype of the cells at the tips of branching airways is unclear from these experiments.

Cells at the tips of branching saccular airways are typically cuboidal, with appearance of flattened, type I cells occurring once branching is complete. Interestingly, NM II isoform expression is prominent in flattened, type I cells by confocal microscopy. Components of type I cell junctions are critical for maintaining a dry alveolar space free of potential barriers to gas exchange (Mitchell et al., 2011). The abundant expression of NM II-A and NM II-C in P0 type I epithelial cells suggests NM II may play a key role in regulating type I cell function and alveolar permeability.

Several pieces of evidence suggest that NM II activity suppresses airway epithelial migration. Blebbistatin caused large changes in cell shape and anisotropy in epithelial cells lining the stalks of airways. Migration and displacement of these cells along the airway stalk is thought to be minimal during development (Bellusci et al., 1997; Park et al., 1998). The blebbistatin-induced increase in airway formation further suggests NM II limits branch formation. Blebbistatin had no effect on cell orientation at the airway tips, where epithelial cells actively migrate in response to chemoattractant factors. Finally, blebbistatin increased the velocity of MLE-12 cells migrating into artificial wounds, demonstrating that NM II restricts cell movement. These data are consistent with previous findings showing that NM II restricts neuronal migration during growth cone guidance (Schaar and McConnell, 2005), and that NM II inhibition facilitates extension of endothelial cell pseudopodia during angiogenesis (Fischer et al., 2009). Studies in cultured fibroblasts also showed that NM II recruits vinculin to areas of focal contact formation, stabilizing the focal contacts and limiting cell migration, while blebbistatin allowed focal contact dissolution and increased migration (Dumbauld et al., 2010; Pasapera et al., 2010). In the case of airway branching, NM II may act to limit epithelial cell movement except at areas where migration is required to form new branches or airway divisions.

Non-muscle myosins clearly play a key role in the morphogenesis of many tissues throughout biology. The actin and myosin cytoskeleton controls convergence extension, tube elongation, and directional cell division (Skoglund et al., 2008; Reed et al., 2009; Yamamoto et al., 2009; Pollard, 2010). Many of the key components of the planar cell polarity machinery characterized in *Drosophila* and *C. elegans* also play important roles in mammalian tissue morphogenesis (Klein and Mlodzik, 2005). However, how planar cell polarity regulates lung morphogenesis and specifically how planar polarity changes during later stages of lung development is unclear. Knockout studies in mice have shown that the planar cell polarity components Celsr1 and Vangl2 are required for normal lung morphogenesis (Yates et al., 2010). Mice lacking either of these genes develop misshapen lung lobes with fewer airways. Celsr1 and Vangl2 are also critical for epithelial integrity and are required to form new epithelial tubes in response to chemoattractants such as FGF-10. Spatial and temporal regulation of planar cell polarity and actinomyosin function contribute to airway morphogenesis, and may play a role in determining the sites of branch formation. Expression of mesenchymal growth factors including FGF-10 is spatially restricted (Bellusci et al., 1997; Park et al., 1998), which could concentrate activation of unique epithelial signals in specific sites. Alternatively, epithelial cells at the tips of airways could produce proteases that degrade components of the extracellular matrix, changing the dynamics of integrin-mediated focal contacts, promoting cell migration and epithelial tube elongation.

Alterations in airway size during development and adult life may play important roles in lung disease pathogenesis. Patients with cystic fibrosis are born with smaller diameter tracheas, a subtle anomaly that could produce clinically significant airway obstruction (Meyerholz et al., 2010). Neonates born with congenital diaphragmatic hernia also have reduced airway size and branching (Reale and Esterly, 1973; Nose et al., 2000). Respiratory viral infection may cause airway narrowing at the level of the terminal bronchioles, causing significant airflow obstruction and possibly contributing to asthma pathogenesis (Kraft,

1999; Takeda et al., 2010). In older adults, inflammation-mediated changes in airway diameter may play a key role in chronic obstructive pulmonary disease and emphysema (McDonough et al., 2011). Collectively, these clinical pieces of evidence support the importance of proper maintenance of airway caliber during development and in the mature airway following injury. Determining the role of specific molecular components of the epithelial cytoskeleton in development and disease processes may provide insight into new therapeutic opportunities.

Experimental Procedures

Whole lung lobe preparation and e-cadherin immunostaining

Fetal lung lobes were harvested from E15, E16, and E17 timed pregnant wild type C57BL/6J mice (Jackson Laboratory). All animal protocols and procedures were reviewed and approved by the Vanderbilt Institutional Animal Care and Use Committee. Lung lobes were dissected free from surrounding tissue, fixed in 4% paraformaldehyde for 40 min at room temperature, permeabilized with 0.1% Triton X-100, and immunostained with rat anti-E-cadherin (Invitrogen). Alexa-conjugated secondary antibodies were used for fluorescent detection (Invitrogen). Immunostained lobes were mounted in ProLong Gold using a nylon spacer and imaged using a Leica TCS SPE-2 laser scanning confocal microscope. For epithelial orientation, images were acquired at the very tips of airways at the lung periphery. Only airways perpendicular to the plane of imaging were imaged.

Frozen section preparation and myosin immunostaining

For immunostaining of NM IIA, IIB, and IIC, fetal mouse lung lobes were harvested at E15, E18, and P0. The lobes were processed through sucrose gradients, frozen in OCT, and cut in 8 μm sections. Frozen sections were fixed in 2% paraformaldehyde for 20 min at room temperature, permeabilized with 0.1% Triton X-100, and immunostained with antibodies against E-cadherin (Invitrogen), myosin IIA (Abcam), myosin IIB (Covance), and myosin IIC (Abcam). Wild type E18 fetal mouse lungs were similarly processed and immunostained with antibodies against T1α (Developmental Studies Hybridoma Bank at the University of Iowa) and NKX2-1 (Santa Cruz Biotechnology). Alexa-conjugated secondary antibodies were used for fluorescent detection (Invitrogen). Immunostained sections were mounted in ProLong Gold (Invitrogen) and imaged using laser scanning confocal microscopy.

Fetal lung explant culture and imaging

Lung explants from E15 C57BL/6J mice were cultured on permeable supports and an air-liquid interface at 37° in 95 % air/5% CO_2 (Prince et al., 2004; Prince et al., 2005; Dieperink et al., 2006; Benjamin et al., 2007; Benjamin et al., 2009; Benjamin et al., 2010; Blackwell et al., 2011). All explants were cultured under control conditions overnight to allow the explants to seal and adhere to the permeable support. Control and experimental explants were imaged at 0 h, 4 h, and 18 h following blebbistatin treatment (100 μM, Cayman Chemical Company). To quantify new branch formation, the number of airways along the periphery of each explant was measured in control and blebbistatin explants at 0, 4, and 18 hours following treatment. For each experimental replicate, at least 5 randomly oriented explants were studied at each time point and condition. ImageJ was used to measure the peripheral airway size of 10 consecutive peripheral airways per explant (consecutive airways chosen clockwise from 12:00 position). Similarly, the average epithelial cell size was calculated from the area of the first 10 consecutive peripheral airways (clockwise from 12:00 position) divided by the total number of epithelial cells present in each airway. The Degree of Anisotropy was calculated on a 153 μm *z*-stack of images using the BoneJ plug-in within ImageJ. Images were acquired from the stalk and tip regions of E-cadherin-immunostained, control and blebbistatin-treated explants. After conversion to a binary

image, the degree of anisotropy was calculated using BoneJ (Odgaard, 1997; Doube et al., 2010). Within this program, the Degree of Anisotropy was calculated using the mean intercept length (MIL). From each *z*-stack, 1000 vectors were generated, each originating from a random point. The MIL for each vector was calculated as the vector length divided by the number of intercepts.

MIL = vector length/ number of intercepts

Next, a vector cloud was generated from the MIL with each endpoint on the vector cloud equal to the vector multiplied by the MIL.

Endpoint vector = vector × MIL

From the vector cloud, a best fit ellipsoid was created. The Degree of Anisotropy was calculated from the best fit ellipsoid as follows:

DA = 1 − (length of shortest axis/length of longest axis)

Within each *z*-stack in stalk and tip regions, the mean Degree of Anisotropy was calculated from 10 separate random points. For comparison of epithelial cell orientations at the tips of airways, explants were treated with blebbistatin for 18 h and immunostained with E-cadherin. Confocal microscopy captured images of the distal tip of airways perpendicular to the plane of imaging. To evaluate the effect of blebbistatin on epithelial cell proliferation, control and 18 h blebbistatin treated explants were immunostained for phospho-histone H3 (PH3) and the percentage of PH3 positive cells was determined from 40x images of consecutive peripheral airways. To test the role of blebbistatin in type I and type II epithelial cell differentiation, control and 18 h blebbistatin treated explants were immunostained for the type I cell marker T1α and the type II cell marker NKX2-1. Although there was minimal T1α expression in these E15 cultured explants, occasional epithelial cells were NKX2-1 positive, quantified by the number of NKX2-1 positive cells per mm^2 in random, non-overlapping 10x confocal images. Data from control and blebbistatin treated explants were compared using a two-tailed t test.

MLE-12 cell culture, wound assay, and immunostaining

MLE-12 cells were grown in RPMI with 10% FBS. For testing migration in a linear wound assay, cells were grown to confluence in 6-well plates, wounded with a 200 μl pipet tip in an identical orientation. Following wounding, cells were washed with serum-free media and placed in RPMI with 1% FBS and heparin (10 μg/ml, Sigma) with and without blebbistatin (1 μm) and FGF-10 (250 ng/ml, R&D Systems). Plates were placed in a stage-top incubator (37 °C, 5% CO2, 95% air; OKO Lab) for live cell imaging using an inverted microscope (Olympus) and CCD camera (Hamamatsu). Images were acquired every 20 min for 8 h. Three separate areas along the wound were imaged in each well, and the entire experiment was repeated three times. For cell velocity measurement, 40 cells along the wound edge were tracked over time using ImageJ. For immunostaining, MLE-12 cells were first grown to confluence on gelatin-coated coverslips, wounded as above, fixed, permeabilized, and labeled using FITC-conjugated anti-tubulin (Sigma), FITC-conjugated anti-phospho-tyrosine (Millipore), or Alexa594-conjugated phalloidin (Invitrogen). Nuclei were labeled with Hoescht dye and cells were imaged using a wide-field fluorescence microscope (Olympus) with a monochrome CCD camera (Hamamatsu) and Slidebook software.

Acknowledgments

The authors would like to thank Amanda Im, Riet van der Meer, and Jin-Hua Liu for their outstanding technical assistance. Special thanks to Jeff Reese, Timothy Blackwell, Scott Baldwin, Candice Fike, Scott Weiss, and Alvin Kho for helpful comments and ideas regarding both this project and the manuscript. The Vanderbilt Cell Imaging Shared Resource Center is supported by the NIH (CA68485, DK20593, DK58404, HD15052, DK59637,

EY08126). This work was supported by the March of Dimes (5FY07-555 L.S.P.), the NIH (HL097195 L.S.P., HL086324 L.S.P., HD060554 E.J.P.), an Ikaria Advancing Newborn Medicine Fellowship Grant (E.J.P.), and the Marshall Klaus Perinatal Research Award from the American Academy of Pediatrics (E.J.P.).

References

Affolter M, Bellusci S, Itoh N, Shilo B, Thiery JP, Werb Z. Tube or not tube: remodeling epithelial tissues by branching morphogenesis. Dev Cell. 2003; 4:11–18. [PubMed: 12530959]

Bellusci S, Grindley J, Emoto H, Itoh N, Hogan BL. Fibroblast growth factor 10 (FGF10) and branching morphogenesis in the embryonic mouse lung. Development. 1997; 124:4867–4878. [PubMed: 9428423]

Benjamin JT, Carver BJ, Plosa EJ, Yamamoto Y, Miller JD, Liu JH, van der Meer R, Blackwell TS, Prince LS. NF-kappaB activation limits airway branching through inhibition of Sp1-mediated fibroblast growth factor-10 expression. J Immunol. 2010; 185:4896–4903. [PubMed: 20861353]

Benjamin JT, Gaston DC, Halloran BA, Schnapp LM, Zent R, Prince LS. The role of integrin alpha8beta1 in fetal lung morphogenesis and injury. Dev Biol. 2009; 335:407–417. [PubMed: 19769957]

Benjamin JT, Smith RJ, Halloran BA, Day TJ, Kelly DR, Prince LS. FGF-10 is decreased in bronchopulmonary dysplasia and suppressed by Toll-like receptor activation. Am J Physiol Lung Cell Mol Physiol. 2007; 292:L550–L558. [PubMed: 17071719]

Betapudi V, Licate LS, Egelhoff TT. Distinct roles of nonmuscle myosin II isoforms in the regulation of MDA-MB-231 breast cancer cell spreading and migration. Cancer Res. 2006; 66:4725–4733. [PubMed: 16651425]

Blackwell TS, Hipps AN, Yamamoto Y, Han W, Barham WJ, Ostrowski MC, Yull FE, Prince LS. NF-kappaB signaling in fetal lung macrophages disrupts airway morphogenesis. J Immunol. 2011; 187:2740–2747. [PubMed: 21775686]

Burri PH. Fetal and postnatal development of the lung. Annu Rev Physiol. 1984; 46:617–628. [PubMed: 6370120]

Cao X, Surma MA, Simons K. Polarized sorting and trafficking in epithelial cells. Cell Res. 2012; 22:793–805. [PubMed: 22525333]

Cardoso WV. Lung morphogenesis revisited: old facts, current ideas. Dev Dyn. 2000; 219:121–130. [PubMed: 11002333]

Cho YS, Stevens LM, Sieverman KJ, Nguyen J, Stein D. A Ventrally Localized Protease in the Drosophila Egg Controls Embryo Dorsoventral Polarity. Curr Biol. 2012

Christou H, Brodsky D. Lung injury and bronchopulmonary dysplasia in newborn infants. J Intensive Care Med. 2005; 20:76–87. [PubMed: 15855220]

Conti MA, Even-Ram S, Liu C, Yamada KM, Adelstein RS. Defects in cell adhesion and the visceral endoderm following ablation of nonmuscle myosin heavy chain II-A in mice. J Biol Chem. 2004; 279:41263–41266. [PubMed: 15292239]

Dieperink HI, Blackwell TS, Prince LS. Hyperoxia and apoptosis in developing mouse lung mesenchyme. Pediatr Res. 2006; 59:185–190. [PubMed: 16439576]

Doube M, Klosowski MM, Arganda-Carreras I, Cordelieres FP, Dougherty RP, Jackson JS, Schmid B, Hutchinson JR, Shefelbine SJ. BoneJ: Free and extensible bone image analysis in ImageJ. Bone. 2010; 47:1076–1079. [PubMed: 20817052]

Dumbauld DW, Shin H, Gallant ND, Michael KE, Radhakrishna H, Garcia AJ. Contractility modulates cell adhesion strengthening through focal adhesion kinase and assembly of vinculin-containing focal adhesions. J Cell Physiol. 2010; 223:746–756. [PubMed: 20205236]

Fischer RS, Gardel M, Ma X, Adelstein RS, Waterman CM. Local cortical tension by myosin II guides 3D endothelial cell branching. Curr Biol. 2009; 19:260–265. [PubMed: 19185493]

Golomb E, Ma X, Jana SS, Preston YA, Kawamoto S, Shoham NG, Goldin E, Conti MA, Sellers JR, Adelstein RS. Identification and characterization of nonmuscle myosin II-C, a new member of the myosin II family. J Biol Chem. 2004; 279:2800–2808. [PubMed: 14594953]

Green KJ, Getsios S, Troyanovsky S, Godsel LM. Intercellular junction assembly, dynamics, and homeostasis. Cold Spring Harb Perspect Biol. 2010; 2:a000125. [PubMed: 20182611]

Hogan BL. Morphogenesis. Cell. 1999; 96:225–233. [PubMed: 9988217]

Ivanov AI, Hopkins AM, Brown GT, Gerner-Smidt K, Babbin BA, Parkos CA, Nusrat A. Myosin II regulates the shape of three-dimensional intestinal epithelial cysts. J Cell Sci. 2008; 121:1803–1814. [PubMed: 18460584]

Klein TJ, Mlodzik M. Planar cell polarization: an emerging model points in the right direction. Annu Rev Cell Dev Biol. 2005; 21:155–176. [PubMed: 16212491]

Kollins KM, Hu J, Bridgman PC, Huang YQ, Gallo G. Myosin-II negatively regulates minor process extension and the temporal development of neuronal polarity. Dev Neurobiol. 2009; 69:279–298. [PubMed: 19224562]

Kraft M. The distal airways: are they important in asthma? Eur Respir J. 1999; 14:1403–1417. [PubMed: 10624774]

Larsen M, Hoffman MP, Sakai T, Neibaur JC, Mitchell JM, Yamada KM. Role of PI 3-kinase and PIP3 in submandibular gland branching morphogenesis. Dev Biol. 2003; 255:178–191. [PubMed: 12618142]

Lawrence PA, Shelton PM. The determination of polarity in the developing insect retina. J Embryol Exp Morphol. 1975; 33:471–486. [PubMed: 1176856]

Limouze J, Straight AF, Mitchison T, Sellers JR. Specificity of blebbistatin, an inhibitor of myosin II. J Muscle Res Cell Motil. 2004; 25:337–341. [PubMed: 15548862]

Lo CM, Buxton DB, Chua GC, Dembo M, Adelstein RS, Wang YL. Nonmuscle myosin IIb is involved in the guidance of fibroblast migration. Mol Biol Cell. 2004; 15:982–989. [PubMed: 14699073]

Ma X, Jana SS, Conti MA, Kawamoto S, Claycomb WC, Adelstein RS. Ablation of nonmuscle myosin II-B and II-C reveals a role for nonmuscle myosin II in cardiac myocyte karyokinesis. Mol Biol Cell. 2010; 21:3952–3962. [PubMed: 20861308]

MacDorman MF, Martin JA, Mathews TJ, Hoyert DL, Ventura SJ. Explaining the 2001-02 infant mortality increase: data from the linked birth/infant death data set. Natl Vital Stat Rep. 2005; 53:1–22. [PubMed: 15712582]

Mathews TJ, MacDorman MF. Infant mortality statistics from the 2007 period linked birth/infant death data set. Natl Vital Stat Rep. 2011; 59:1–30.

McDonough JE, Yuan R, Suzuki M, Seyednejad N, Elliott WM, Sanchez PG, Wright AC, Gefter WB, Litzky L, Coxson HO, Pare PD, Sin DD, Pierce RA, Woods JC, McWilliams AM, Mayo JR, Lam SC, Cooper JD, Hogg JC. Small-airway obstruction and emphysema in chronic obstructive pulmonary disease. N Engl J Med. 2011; 365:1567–1575. [PubMed: 22029978]

Mercer RR, Russell ML, Roggli VL, Crapo JD. Cell number and distribution in human and rat airways. Am J Respir Cell Mol Biol. 1994; 10:613–624. [PubMed: 8003339]

Metzger RJ, Klein OD, Martin GR, Krasnow MA. The branching programme of mouse lung development. Nature. 2008; 453:745–750. [PubMed: 18463632]

Meyerholz DK, Stoltz DA, Namati E, Ramachandran S, Pezzulo AA, Smith AR, Rector MV, Suter MJ, Kao S, McLennan G, Tearney GJ, Zabner J, McCray PB Jr, Welsh MJ. Loss of cystic fibrosis transmembrane conductance regulator function produces abnormalities in tracheal development in neonatal pigs and young children. Am J Respir Crit Care Med. 2010; 182:1251–1261. [PubMed: 20622026]

Mitchell LA, Overgaard CE, Ward C, Margulies SS, Koval M. Differential effects of claudin-3 and claudin-4 on alveolar epithelial barrier function. Am J Physiol Lung Cell Mol Physiol. 2011; 301:L40–L49. [PubMed: 21515662]

Nose K, Kamata S, Sawai T, Tazuke Y, Usui N, Kawahara H, Okada A. Airway anomalies in patients with congenital diaphragmatic hernia. J Pediatr Surg. 2000; 35:1562–1565. [PubMed: 11083423]

Odgaard A. Three-dimensional methods for quantification of cancellous bone architecture. Bone. 1997; 20:315–328. [PubMed: 9108351]

Park WY, Miranda B, Lebeche D, Hashimoto G, Cardoso WV. FGF-10 is a chemotactic factor for distal epithelial buds during lung development. Dev Biol. 1998; 201:125–134. [PubMed: 9740653]

Pasapera AM, Schneider IC, Rericha E, Schlaepfer DD, Waterman CM. Myosin II activity regulates vinculin recruitment to focal adhesions through FAK-mediated paxillin phosphorylation. J Cell Biol. 2010; 188:877–890. [PubMed: 20308429]

Pollard TD. Mechanics of cytokinesis in eukaryotes. Curr Opin Cell Biol. 2010; 22:50–56. [PubMed: 20031383]

Prince LS, Dieperink HI, Okoh VO, Fierro-Perez GA, Lallone RL. Toll-like receptor signaling inhibits structural development of the distal fetal mouse lung. Dev Dyn. 2005; 233:553–561. [PubMed: 15830384]

Prince LS, Okoh VO, Moninger TO, Matalon S. Lipopolysaccharide increases alveolar type II cell number in fetal mouse lungs through Toll-like receptor 4 and NF-kappaB. Am J Physiol Lung Cell Mol Physiol. 2004; 287:L999–L1006. [PubMed: 15475494]

Reale FR, Esterly JR. Pulmonary hypoplasia: a morphometric study of the lungs of infants with diaphragmatic hernia, anencephaly, and renal malformations. Pediatrics. 1973; 51:91–96. [PubMed: 4684452]

Reed RA, Womble MA, Dush MK, Tull RR, Bloom SK, Morckel AR, Devlin EW, Nascone-Yoder NM. Morphogenesis of the primitive gut tube is generated by Rho/ROCK/myosin II-mediated endoderm rearrangements. Dev Dyn. 2009; 238:3111–3125. [PubMed: 19924810]

Schaar BT, McConnell SK. Cytoskeletal coordination during neuronal migration. Proc Natl Acad Sci U S A. 2005; 102:13652–13657. [PubMed: 16174753]

Schreider JP, Raabe OG. Structure of the human respiratory acinus. Am J Anat. 1981; 162:221–232. [PubMed: 7315750]

Skoglund P, Rolo A, Chen X, Gumbiner BM, Keller R. Convergence and extension at gastrulation require a myosin IIB-dependent cortical actin network. Development. 2008; 135:2435–2444. [PubMed: 18550716]

Srinivas S, Goldberg MR, Watanabe T, D'Agati V, al-Awqati Q, Costantini F. Expression of green fluorescent protein in the ureteric bud of transgenic mice: a new tool for the analysis of ureteric bud morphogenesis. Dev Genet. 1999; 24:241–251. [PubMed: 10322632]

Straight AF, Cheung A, Limouze J, Chen I, Westwood NJ, Sellers JR, Mitchison TJ. Dissecting temporal and spatial control of cytokinesis with a myosin II Inhibitor. Science. 2003; 299:1743–1747. [PubMed: 12637748]

Takeda K, Kishi H, Ma X, Yu ZX, Adelstein RS. Ablation and mutation of nonmuscle myosin heavy chain II-B results in a defect in cardiac myocyte cytokinesis. Circ Res. 2003; 93:330–337. [PubMed: 12893741]

Takeda T, Oga T, Niimi A, Matsumoto H, Ito I, Yamaguchi M, Matsuoka H, Jinnai M, Otsuka K, Oguma T, Nakaji H, Chin K, Mishima M. Relationship between small airway function and health status, dyspnea and disease control in asthma. Respiration. 2010; 80:120–126. [PubMed: 19776554]

Ten Have-Opbroek AA. The development of the lung in mammals: an analysis of concepts and findings. Am J Anat. 1981; 162:201–219. [PubMed: 7032272]

Tian X, Liu Z, Niu B, Zhang J, Tan TK, Lee SR, Zhao Y, Harris DC, Zheng G. E-cadherin/beta-catenin complex and the epithelial barrier. J Biomed Biotechnol. 2011; 2011:567305. [PubMed: 22007144]

Veltmaat JM, Mailleux AA, Thiery JP, Bellusci S. Mouse embryonic mammogenesis as a model for the molecular regulation of pattern formation. Differentiation. 2003; 71:1–17. [PubMed: 12558599]

Vicente-Manzanares M, Ma X, Adelstein RS, Horwitz AR. Non-muscle myosin II takes centre stage in cell adhesion and migration. Nat Rev Mol Cell Biol. 2009; 10:778–790. [PubMed: 19851336]

Vicente-Manzanares M, Webb DJ, Horwitz AR. Cell migration at a glance. J Cell Sci. 2005; 118:4917–4919. [PubMed: 16254237]

Vicente-Manzanares M, Zareno J, Whitmore L, Choi CK, Horwitz AF. Regulation of protrusion, adhesion dynamics, and polarity by myosins IIA and IIB in migrating cells. J Cell Biol. 2007; 176:573–580. [PubMed: 17312025]

Vinson CR, Adler PN. Directional non-cell autonomy and the transmission of polarity information by the frizzled gene of Drosophila. Nature. 1987; 329:549–551. [PubMed: 3116434]

Wang A, Ma X, Conti MA, Adelstein RS. Distinct and redundant roles of the non-muscle myosin II isoforms and functional domains. Biochem Soc Trans. 2011; 39:1131–1135. [PubMed: 21936777]

Wang H, Tewari A, Einheber S, Salzer JL, Melendez-Vasquez CV. Myosin II has distinct functions in PNS and CNS myelin sheath formation. J Cell Biol. 2008; 182:1171–1184. [PubMed: 18794332]

Watanabe T, Costantini F. Real-time analysis of ureteric bud branching morphogenesis in vitro. Dev Biol. 2004; 271:98–108. [PubMed: 15196953]

Wylie SR, Chantler PD. Myosin IIC: a third molecular motor driving neuronal dynamics. Mol Biol Cell. 2008; 19:3956–3968. [PubMed: 18614800]

Yam PT, Wilson CA, Ji L, Hebert B, Barnhart EL, Dye NA, Wiseman PW, Danuser G, Theriot JA. Actin-myosin network reorganization breaks symmetry at the cell rear to spontaneously initiate polarized cell motility. J Cell Biol. 2007; 178:1207–1221. [PubMed: 17893245]

Yamamoto N, Okano T, Ma X, Adelstein RS, Kelley MW. Myosin II regulates extension, growth and patterning in the mammalian cochlear duct. Development. 2009; 136:1977–1986. [PubMed: 19439495]

Yates LL, Schnatwinkel C, Murdoch JN, Bogani D, Formstone CJ, Townsend S, Greenfield A, Niswander LA, Dean CH. The PCP genes Celsr1 and Vangl2 are required for normal lung branching morphogenesis. Hum Mol Genet. 2010; 19:2251–2267. [PubMed: 20223754]

Bullet points

- Epithelial cell orientations occur in four predictable orientations; tetrahedral, linear, rosette, and discontinuous
- Non-muscle myosin II-C co-localizes with both alveolar type I and type II epithelial cells
- Inhibition of NM II increases airway branch formation and peripheral airway size
- Inhibition of NM II increases epithelial cell size and anisotropy
- Blebbistatin increases migration of cultured epithelial cells

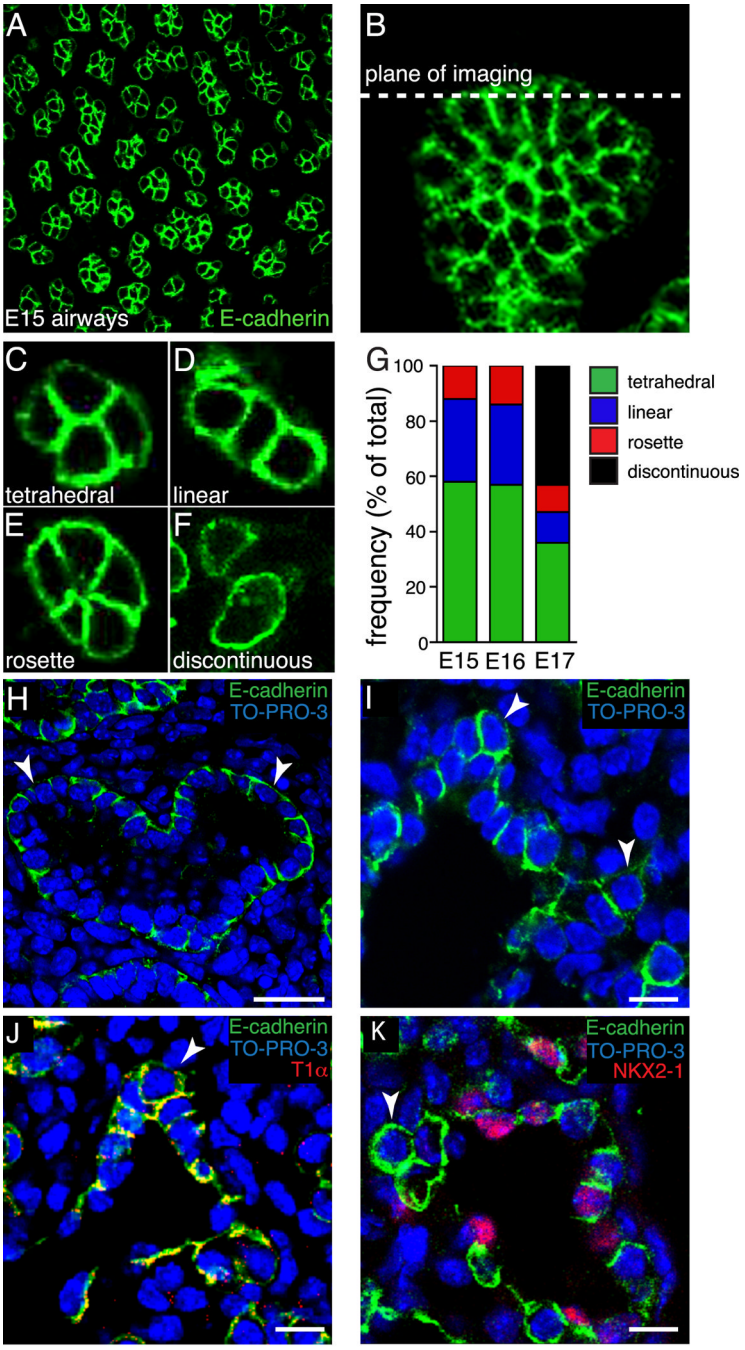

Figure 1.

Epithelial cell orientation at the tips of E15, E16, and E17 fetal mouse lung airways. **(A).** Representative confocal image of E-cadherin expression in E15 mouse whole lung lobe. **(B).** Z-projection of E-cadherin expression in whole lung lobe showing the plane of imaging used for measuring cell orientation. **(C–F)** E-cadherin immunolabeling and confocal imaging revealed four distinct epithelial cell orientations; tetrahedral **(C)**, linear **(D)**, rosette **(E)**, and discontinuous **(F). (G)** Similar frequencies of epithelial orientations in E15 and E16 airways (n = 230, 201, respectively). At E17 (n = 347), over 40% of the airways contained epithelia in a discontinuous orientation, with remaining airways distributed among the three

orientations observed at E15 and E16. **(H, I)**. E-cadherin immunolabeling of E15 mouse lung frozen sections demonstrated distinct epithelial monolayer surrounding the lumen of branched airways **(H)**. E17 epithelial cells at the tips of branching airways (arrowheads) did not maintain a monolayer, but appeared to invade the mesenchyme **(I)**. E18 tip epithelial cells (arrowheads) expressed type I epithelial cell marker, T1α **(J)**, but lacked expression of NKX2-1, type II epithelial cell marker **(K). (H)** Scale bar, 25 μm. **(I–K)** Scale bar, 10 μm.

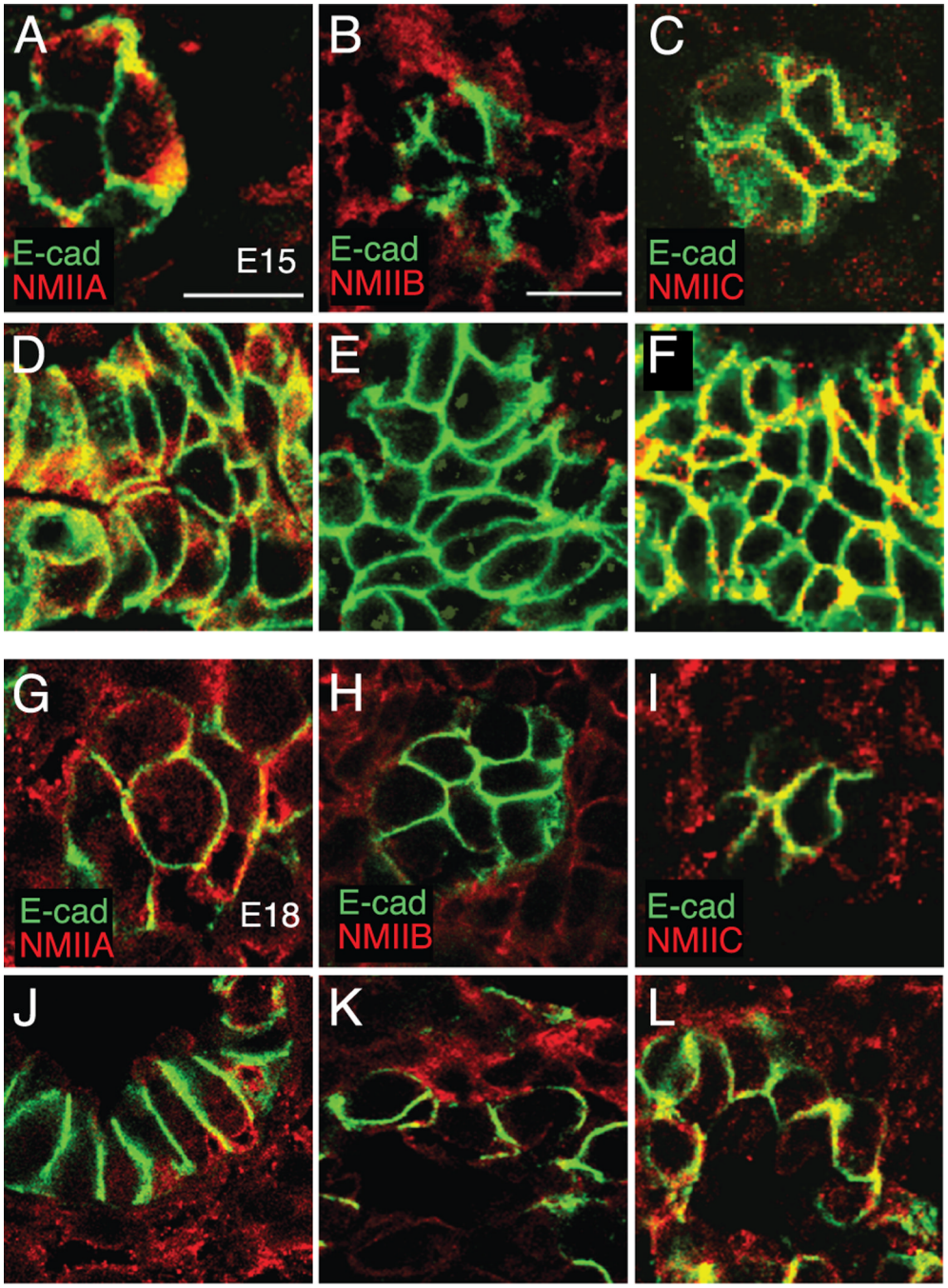

Figure 2.

Non-muscle myosin II (NM II) isoforms are expressed at both airway tips and stalks in developing fetal mouse lung. Confocal images of E15 tip **(A–C)**, E15 stalk **(D–F)**, E18 tip **(G–I)**, and E18 stalk **(J–L)** regions of fetal mouse lungs were immunostained using antibodies against E-cadherin (green) and either NM II-A, NM II-B, or NM II-C (red). **(A, D, G, J)** NM II-A is expressed in fetal mouse lung mesenchyme and epithelium in the tip and stalk regions. **(B, E, H, K)** NM II-B is expressed primarily in the mesenchyme in both the tip and stalk regions at E15 and E18. **(C, F, I, L)** NM II-C co-localizes with E-cadherin in epithelial cells at the tip and stalk regions at E15 and E18. Scale bar, 10 μm.

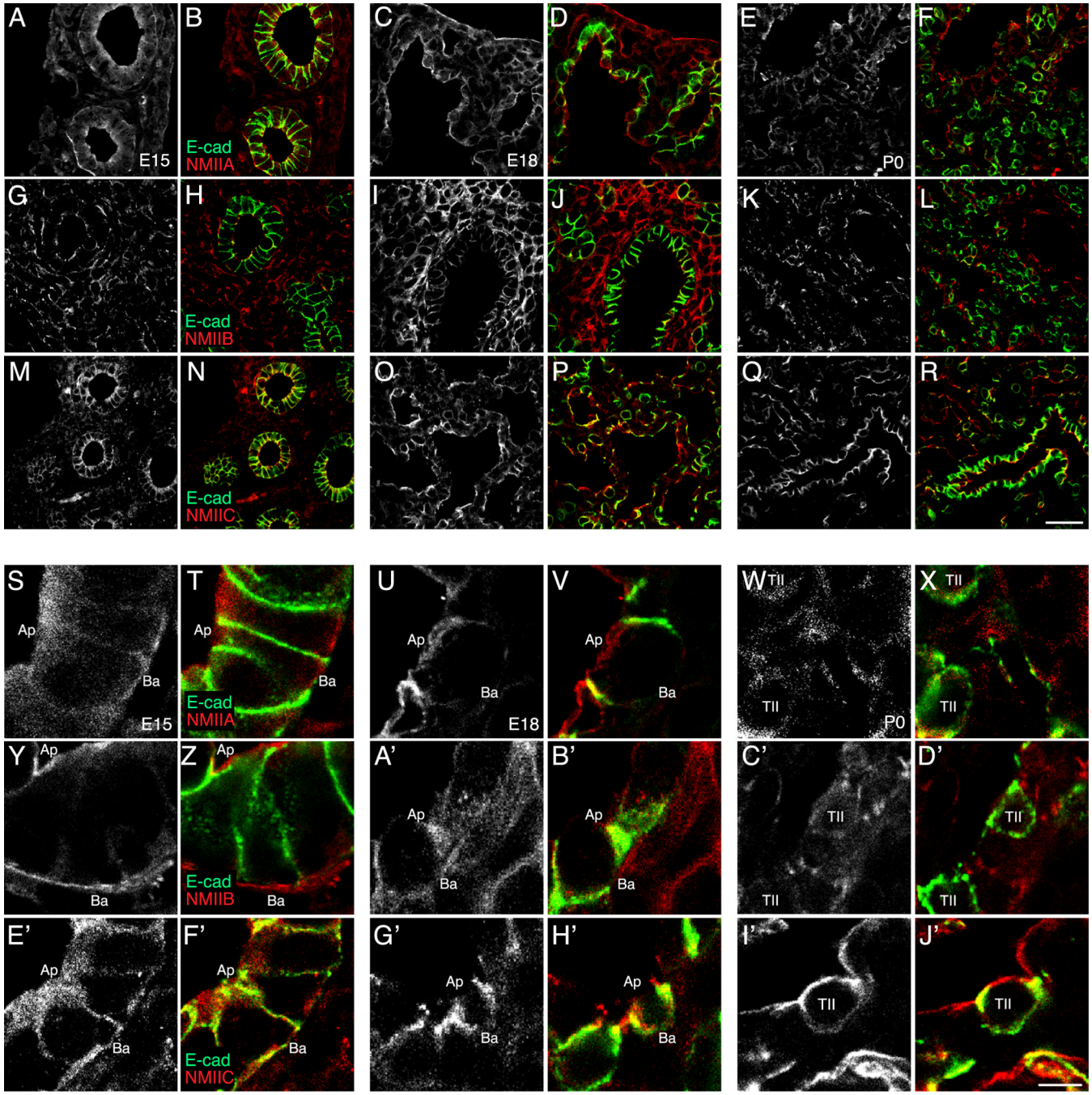

Figure 3.

Non-muscle myosin II (NM II) isoform expression in the developing fetal mouse lung. Confocal images of E15 **(B, H, N, T, Z, F')**, E18 **(D, J, P, V, B', H')**, and P0 **(F, L, R, X, D', J')** mouse lung frozen sections immunostained for E-cadherin (green) and NM II-A, NM II-B, or NM II-C (red). Single channel confocal images of NM II isoform immunostained mouse lung frozen sections at E15 **(A, G, M, S, Y, E')**, E18 **(C, I, O, U, A', G')**, and P0 **(E, K, Q, W, C', I')**. **(A–F, S–X)** NM II-A was present in both the fetal lung mesenchyme and epithelium at E15 and E18, but localized away from type II alveolar epithelial cells at P0. **(G–L, Y–D')** NM II-B localized to the fetal lung mesenchyme. **(M–R, E'–J')** NM II-C co-

localized with E-cadherin along the apical and basolateral surfaces of fetal airway epithelial cells and was expressed in both alveolar type I and type II epithelial cells **(R, J'). (A–R)** Scale bar, 25 μm. **(S–J')** Scale bar, 5 μm.

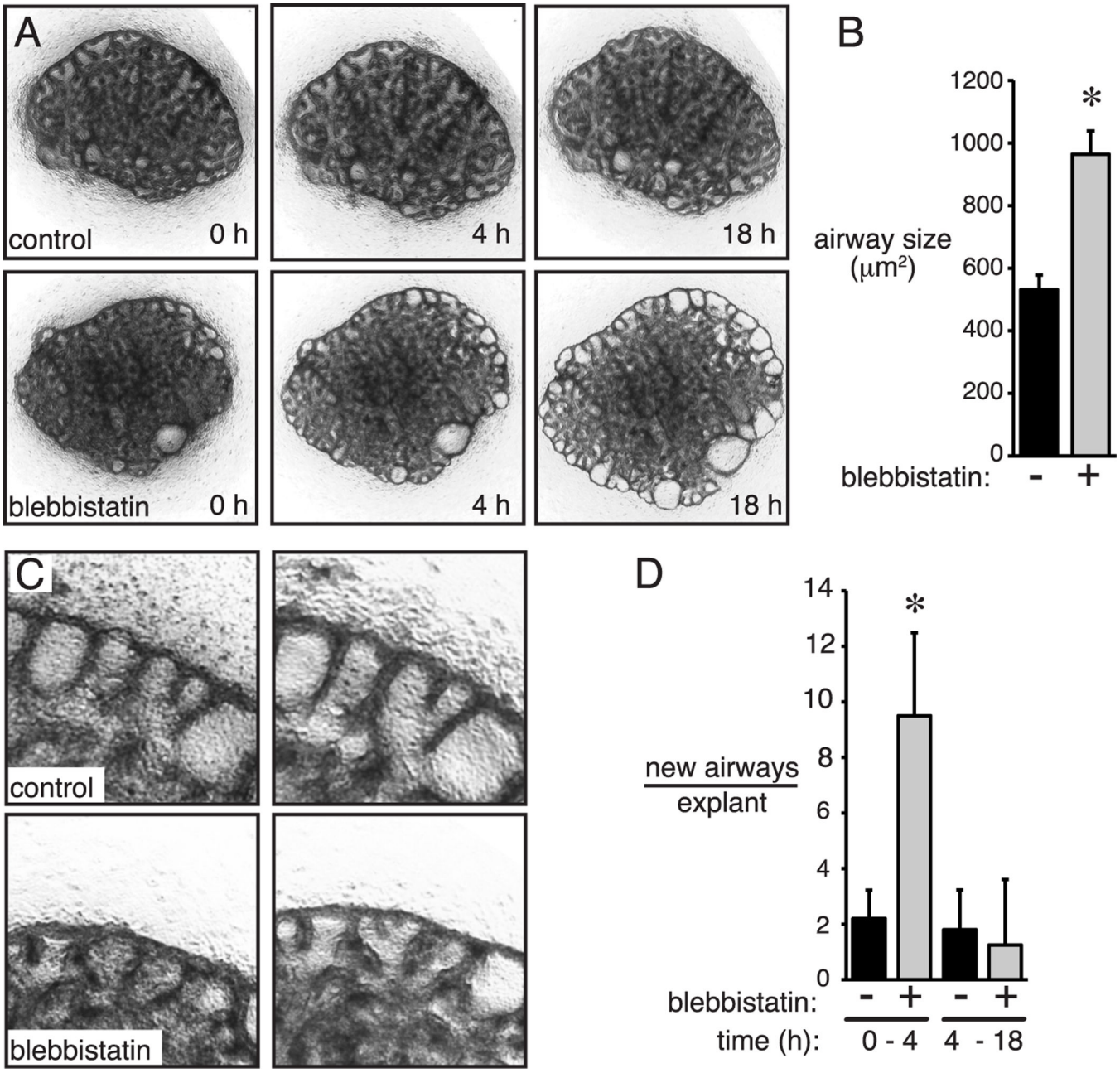

Figure 4.

Non-muscle myosin II inhibition increased airway branching and peripheral airway size. **(A)**. Low power time-lapse images of control and blebbistatin treated explants. Dilated peripheral airways clearly visible by 18 h. (**B**) Blebbistatin increased peripheral airway size by 18 h (* $P < 0.05$, n = 5). **(C, D)** Blebbistatin increased airway branch formation following 4 h of treatment, but had no effect between 4 h and 18 h (* $P < 0.05$, n = 5).

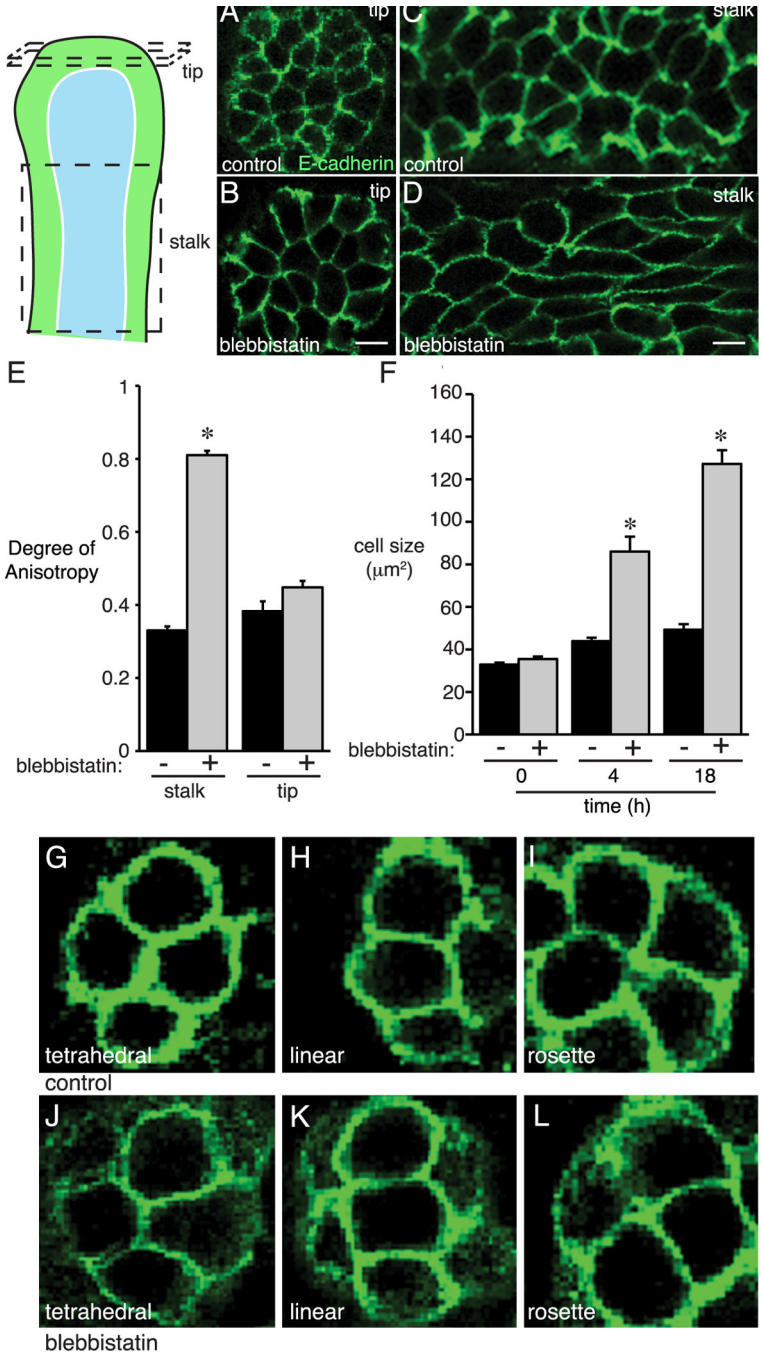

Figure 5.

Blebbistatin increased epithelial cell size and anisotropy. Fetal mouse lung explants were treated with blebbistatin for 4 h or 18 h and then immunostained for E-cadherin. **(A, B)** Epithelial cells at the tips of branching airways had similar orientation and appearance in control and 18 h blebbistatin-treated explants. (**C, D**) Epithelial cells along the airway stalks in 18 h blebbistatin-treated explants appeared longer, more elongated, and displayed disordered orientation. (**E**) Epithelial Degree of Anisotropy was measured in 3-dimensions along the airway stalk and at the airway tip. Blebbistatin increased Degree of Anisotropy along the airway stalk but not at the airway tip. (**F**) Blebbistatin increased epithelial size at

the tips of branching airways at 4 h and 18 h (* $P < 0.05$, n = 110). **(G–L)** Inhibition of non-muscle myosin II did not alter epithelial cell orientation in 18 h blebbistatin treated fetal mouse lung explants. Representative images of epithelial cell orientations in control **(G–I)** and blebbistatin-treated **(J–L)** lung explants.

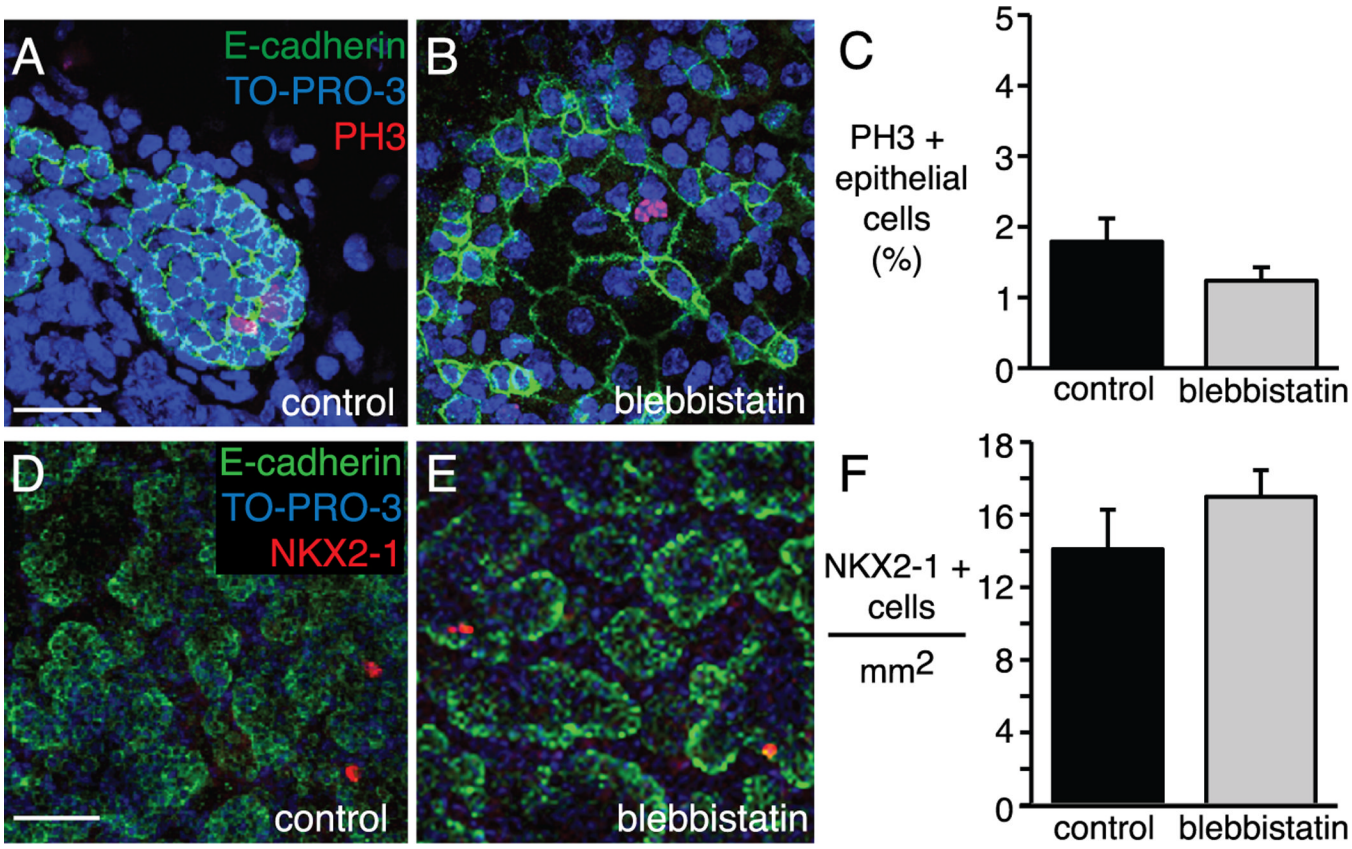

Figure 6.

Inhibition of non-muscle myosin II with blebbistatin did not alter epithelial cell proliferation or differentiation in fetal mouse lung explants. **(A–B)** Control and 18 h blebbistatin treated lung explants immunostained for E-cadherin (green) and the mitotic cell marker PH3 (red). **(C)** The percent of PH3 positive epithelial cells in peripheral airways decreased in blebbistatin treated explants, but was not significant ($P = 0.13$, n = 85 airways). **(D–E)** Confocal images of control and 18 h blebbistatin treated E15 lung explants immunostained for E-cadherin (green) and NKX2-1 (red). Little epithelial cell differentiation was detected at this developmental time point. **(F)** There was no difference in the number of NKX2-1 positive epithelial cells per mm^2 of lung explant. **(A–B)** Scale bar, 50 μm. **(D–E)** Scale bar, 100 μm.

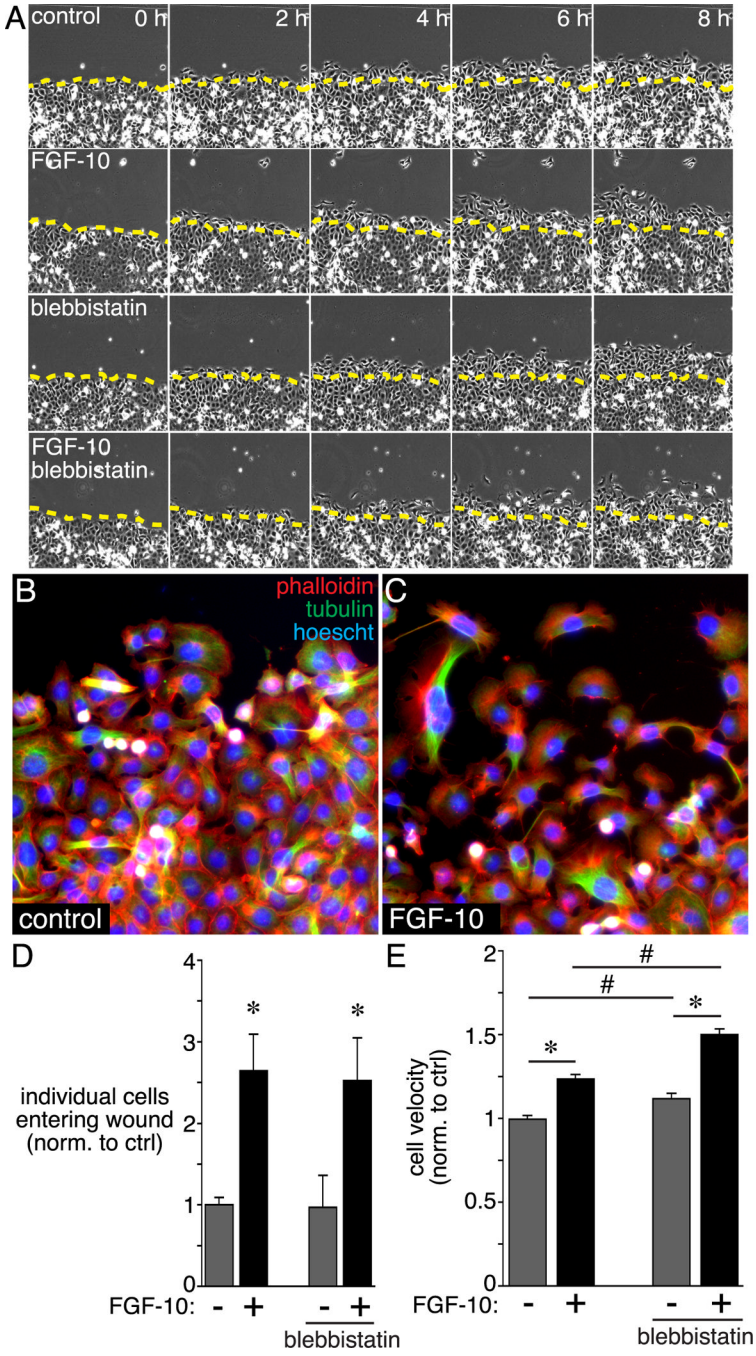

Figure 7.

Effects of blebbistatin on FGF-10-stimulated epithelial cell migration. MLE-12 lung epithelial cells were grown to confluence and then scratched to produce an artificial wound. Following wounding, cells were treated with FGF-10 +/− blebbistatin and imaged by time-lapse microscopy for 8 h. (**A**) Individual still images obtained by phase contrast microscopy show migration of cells into the wound. Images were obtained every 20 min, and representative images from 0 h, 2 h, 4 h, 6 h, and 8 h are shown. (**B, C**) Control and FGF-10 treated MLE-12 cells were labeled with FITC-conjugated anti-tubulin (green) and Alexa594 phalloidin (red) at 8 h following wounding. (**D**) FGF-10 treatment increased the number of

cells migrating into the wound and losing contact with the existing monolayer (* $P < 0.05$, n = 9). Blebbistatin treatment did not have any effect on the number of cells entering the wound. (**E**) FGF-10 increased MLE-12 cell velocity in wounded cultures (* $P < 0.05$, n = 120). Blebbistatin treatment increased velocity in both control and FGF-10-treated cells (# $P < 0.05$, n = 120).

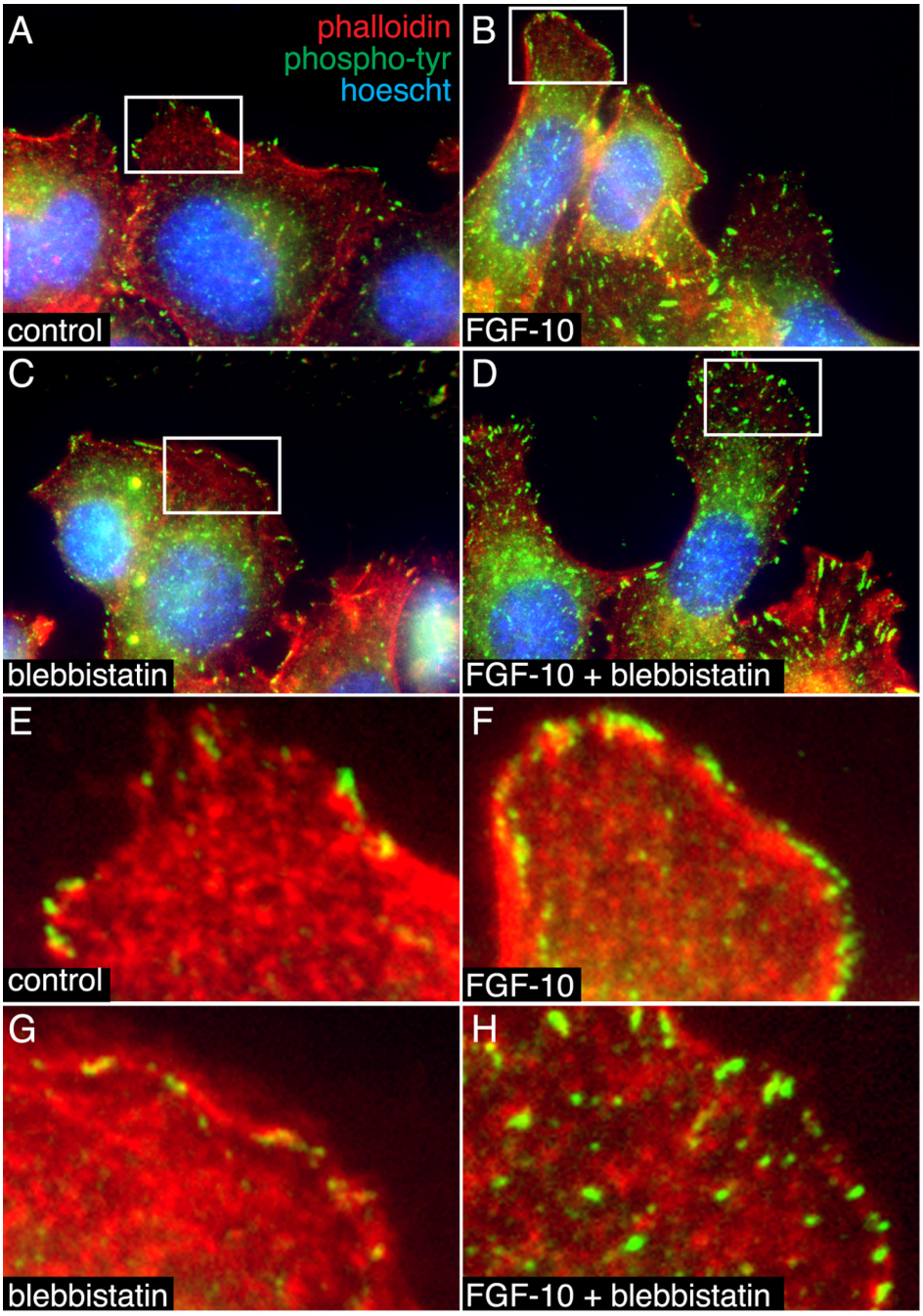

Figure 8.

Blebbistatin altered the subcellular localization of phosphotyrosine staining in MLE-12 cells. **(A–D)**. MLE-12 cells treated with FGF-10 +/− blebbistatin were labeled with FITC-conjugated anti-phophotyrosine (green) and Alexa594-phalloidin (red). Nuclei were labeled with Hoescht dye (blue). (**B**). FGF-10 increased phosphotyrosine staining at the cell periphery. (**C, D**). Blebbistatin decreased the size of phosphotyrosine-positive focal contacts in control cells and caused a more generalized distribution following FGF-10 treatment. Lower magnification images were taken by widefield fluorescence microscopy **(A–D)**.

Higher magnification images obtained by laser scanning confocal microscopy are included in panels (**E–H**).